# Multistage Stretching of High-Density Polyethylene Monofilaments in Melt Spinning

K. YAGI* and C. D. HAN, *Department of Chemical Engineering, Polytechnic Institute of New York, Brooklyn, New York 11201*

## Synopsis

An experimental study was carried out to investigate the influence of molecular weight distribution on stretchability and thread nonuniformity of high-density polyethylene monofilaments. For the study, a melt-spinning/multistage stretching device was constructed, and the monofilaments were extruded first into a quench tank and subsequently stretched twice in an annealing bath. Processing variables investigated were (a) the extrusion temperature, (b) the shear rate in the spinnerette hole, (c) the air-gap distance, (d) the annealing bath temperature, (e) the take-up speed at the first-stage stretching, and (f) the take-up speed at the second-stage stretching. Fiber samples were collected at each stage of stretching, namely, (a) as melt-spun, (b) after the first-stage stretching, and (c) after the second-stage stretching. The maximum stretch rate at which thread breakage occurs was determined at the first- and second-stage stretching in the annealing bath. The melt-spun materials were three different grades of Mitsui Petrochemicals high-density polyethylene and two different grades of Union Carbide high-density polyethylene. Also melt spun were blends of two Mitsui polyethylenes and the two Union Carbide polyethylenes. An attempt was made (a) to correlate stretchability with the molecular weight distribution of the high-density polyethylene; (b) to identify the influence of spinning conditions on stretchability for a given polymer; (c) to correlate the variations of the fiber diameter with the molecular weight distribution and spinning conditions, and (d) to correlate the stretchability of a blend system with blending ratio. tensile properties (the tensile strength at the yield point, tensile elastic modulus, and percent elongation at break) were determined for all fiber samples collected, using the Instron tensile tester. For some fiber samples of special interest, selected on the basis of the spinning experiment results, wide-angle x-ray diffraction measurements were taken to determine the molecular orientation in a filament.

## INTRODUCTION

In the past, a number of investigators have studied the mechanical properties of high-density polyethylene filaments[1-6] and orientation phenomena in polyethylene.[7-10] However, little has been reported about the effect of molecular weight and its distribution on fiber spinnability and on the mechanical properties of high-density polyethylene monofilaments.

It is generally agreed among researchers that the tensile properties of a melt-spun filament can be improved by an increase in molecular orientation, which can be realized by an additional stretching. The additional stretching usually takes place at a temperature below the polymer melting temperature, and this stretching operation is referred to as cold drawing. During cold drawing, changes of fiber morphology occur, influencing the tensile properties of the drawn fiber. Therefore, an investigation of the relationship between the morphological state and the tensile properties of the drawn fiber is of practical importance.

With synthetic macromolecules, it is possible to control the morphological features, such as molecular orientation and crystallinity and hence the properties

* Permanent address: Mitsui Petrochemical Company, Ltd., Tokyo, Japan.

Journal of Applied Polymer Science, Vol. 22, 2553–2571 (1978)

0021-8995/78/0022-2553$01.00

of final products, through the variables of the processing technique. Molecular orientation is intimately related to the mobility of long macromolecules. In turn, the mobility of macromolecules depends on the temperature, and molecular size, and its distribution. Therefore, improvement in the tensile properties of filaments can be explored from the point of view of processing conditions and molecular weight and its distribution.

In the present study, an attempt is made to obtain correlations between the spinning conditions and tensile properties, between the cold-drawing conditions and tensile properties, and between the fiber morphology and tensile properties of high-density polyethylene monofilaments, with particular emphasis on the influence of molecular weight distribution on the tensile properties and morphological features of monofilaments.

## EXPERIMENTAL

The melt-spinning/stretching apparatus was constructed as schematically shown in Figure 1. It consists of a 1-in. extruder, a spinneret, a quench tank, guide rolls, mechanically driven rolls, an annealing bath, and a take-up device. The melt spinning part of the apparatus was electrically heated, and the temperature was controlled with the aid of a Thermistor-regulated controller. The spinneret had a single hole with a diameter of 2 mm. The annealing bath was electrically heated. In most cases, water was used as the heating medium. However, when attempts were made to take photographs of filaments traveling through the annealing bath, vegetable oil was used.

The materials studied were three different grades of Mitsui Petrochemicals high-density polyethylene and two different grades of Union Carbide high-density polyethylene. The molecular characteristics of these materials are given in Table I, and molecular weight distribution curves are given in Figure 2 for Mitsui high-density polyethylenes and in Figure 3 for Union Carbide high-density polyethylenes. Also, blends of two Mitsui high-density polyethylenes and blends of the two Union Carbide high-density polyethylenes were used (see Table I). These materials were chosen for investigating the effect of molecular weight and its distribution on spinnability, tensile properties, and fiber morphology. The rheological properties of the high-density polyethylenes were determined by means of the Han slit rheometer.[11,12] They are given in Figures 4 and 5.

The polyethylene spinning process employed consists of two steps: (1) extrusion and winding and (2) cold drawing in the annealing bath. In the extrusion-winding step, polymer pellets are fed to the barrel of a screw extruder and

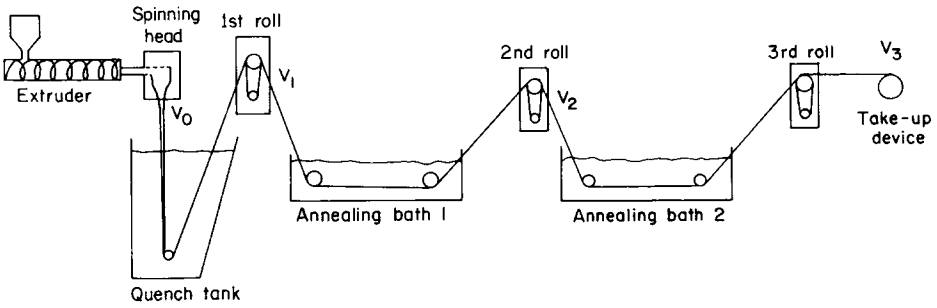


Fig. 1. Schematic of experimental apparatus.

TABLE I
Molecular Characteristics of the High-Density Polyethylenes Used

(a) Homopolymers

| Sample code | Manufacturer | $\overline{M}_n$ | $\overline{M}_w$ |
|---|---|---|---|
| A | Mitsui Petrochemicals | $1.51 \times 10^4$ | $1.51 \times 10^5$ |
| B | Mitsui Petrochemicals | $1.25 \times 10^4$ | $2.43 \times 10^5$ |
| C | Mitsui Petrochemicals | $0.48 \times 10^4$ | $2.26 \times 10^5$ |
| DMDJ 5140 | Union Carbide | $1.33 \times 10^4$ | $1.75 \times 10^5$ |
| DMDJ 4306 | Union Carbide | $0.98 \times 10^4$ | $2.12 \times 10^5$ |

(b) Blends

| Sample code | Blend ratios |
|---|---|
| A/C = 25/75 | 25 wt-%/75 wt-% |
| A/C = 50/50 | 50 wt-%/50 wt-% |
| A/C = 75/25 | 75 wt-%/25 wt-% |
| DMDJ 5140/DMDJ 4306 = 25/75 | 25 wt-%/75 wt-% |
| DMDJ 5140/DMDJ 4306 = 50/50 | 50 wt-%/50 wt-% |
| DMDJ 5140/DMDJ 4306 = 75/25 | 75 wt-%/25 wt-% |

are melted. The melt is transported to the spinning head and extruded through a single-hole spinneret to form a monofilament. The filament leaves the spinneret hole with a velocity $V_0$, which is directly proportional to the volumetric flow rate $Q$, and it enters the quench tank where the cooling of the filament occurs. The filament is pulled by a take-up device with a velocity $V_1$. Hence, the stretch ratio in the melt spinning operation is defined by $V_1/V_0$.

In the cold-drawing step, the filament is fed to the motor-driven roll with a velocity $V_1$ and into the annealing bath (about 6 ft long), in which water (or vegetable oil) is heated electrically. Attenuation and orientation of the filament is realized by pulling the filament with a velocity $V_2$ with the aid of a motor-driven roll placed at the end of the annealing bath. Hence, the stretch ratio in the *first-stage* cold-drawing operation is defined by $V_2/V_1$. After leaving the annealing bath, the same filament is stretched once again in the annealing bath. For the second stretching, the filament velocity is $V_2$ at the take-in rolls and $V_3$

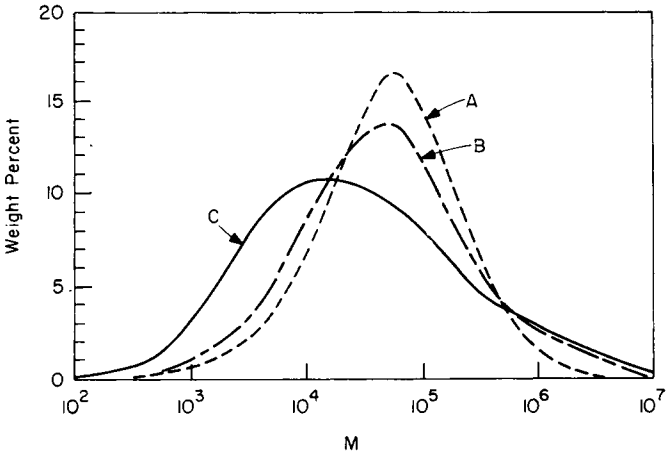


Fig. 2. Molecular weight distribution curve of Mitsui high-density polyethylenes.

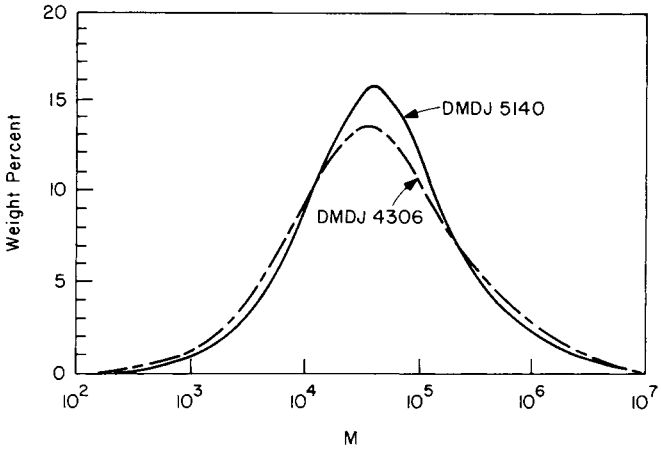


Fig. 3. Molecular weight distribution curve of Union Carbide high-density polyethylenes.

at the take-up rolls. Hence, the stretch ratio in the *second-stage* cold-drawing operation is defined by $V_3/V_1$. (Note that $(V_3/V_2) \times (V_2/V_1) = V_3/V_1$.) The stretch ratio is controlled by adjusting the speed of motors for the take-in and take-up rolls (see Fig. 1).

Processing variables investigated were (1) melt extrusion temperature, (2) melt draw ratio in spinning, (3) air-gap distance in the quench tank, (4) annealing bath temperature, (5) stretch ratio in the annealing bath. At each processing condition, fiber samples were collected for measurements of the tensile properties and fiber morphology. The Instron tensile tester was used for measurement of the tensile properties (the tensile strength at the yield point, tensile elastic modulus, and percent elongation at break), and x-ray diffraction measurements were taken to determine the molecular orientation.

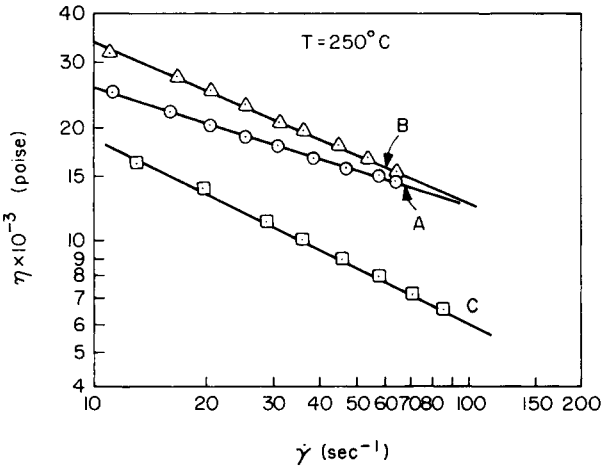


Fig. 4. Viscosity vs shear rate for Mitsui high-density polyethylenes.

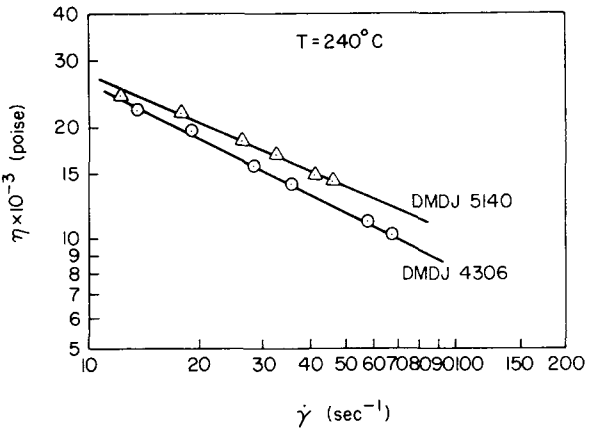


Fig. 5. Viscosity vs shear rate for Union Carbide high-density polyethylenes.

## RESULTS AND DISCUSSION

### The Influence of Molecular Weight Distribution on Stretchability

Table II gives a summary of the cold-drawing operation in terms of the maximum stretch ratio for three different grades of Mitsui high-density polyethylene (HDPE). Note that two stages of cold drawing were performed in order to find out whether or not, after the first stage, an additional cold stretching would improve the tensile properties of the filaments. As can be seen, the maximum stretch ratio is indeed improved by second-stage stretching. This is quite evident for sample A.

Of particular interest in Table II is the effect of molecular weight distribution (MWD) on the maximum stretch ratio $V_3/V_1$. It is seen that the maximum stretch ratio, i.e., stretchability (and hence drawability), is improved as the MWD becomes narrow (see Fig. 2). A similar observation has been reported earlier by Han and Lamonte.[13] Thus, the drawability of the three resins may be ordered in the sequence: sample A > sample B > sample C.

Table III gives a summary of the cold-drawing operations for two Mitsui resins, A and C, at different melt extrusion temperatures. Melt extrusion temperature is seen to have little effect on stretchability in the cold-drawing process. It is worth mentioning that the extrusion at 290°C generated some polymer degradation, which was detected by odor. The particularly low value $(V_3/V_1)_{max}$ for sample A at 290°C may be attributable to the degradation of polymer.

The effect of annealing bath temperature on the maximum stretch ratio was investigated, and the result is summarized in Table IV. The effect of annealing bath temperature on the maximum stretch ratio (i.e., drawability) is not clear.

TABLE II
Summary of the Cold-Drawing Operation of Mitsui High-Density Polyethylenes[a]

| Maximum stretch ratio | Sample A | Sample B | Sample C |
|---|---|---|---|
| 1st stage, $(V_2/V_1)_{max}$ | 10.89 | 10.71 | 8.84 |
| 2nd stage, $(V_3/V_1)_{max}$ | 18.53 | 12.26 | 10.22 |

[a] Other processing conditions: melt-draw ratio ($V_1/V_0$), about 2; air-gap distance, 2 in.; extrusion temperature, 260°C; $V_0$ = 4.83 m/min; annealing bath temperature, 100°C.

TABLE III
The Effect of Melt Extrusion Temperature on the Maximum Stretch Ratio of Mitsui High-Density Polyethylenes[a]

(a) Sample A

| Maximum stretch ratio | Extrusion temperature, °C 250 | 260 | 270 | 290 |
|---|---|---|---|---|
| 1st stage, $(V_2/V_1)_{max}$ | 11.29 | 10.89 | 11.28 | 8.54 |
| 2nd stage, $(V_3/V_1)_{max}$ | 18.70 | 18.53 | 16.11 | 15.64 |

(b) Sample C

| Maximum stretch ratio | Extrusion temperature, °C 240 | 250 | 260 | 270 | 290 |
|---|---|---|---|---|---|
| 1st stage, $(V_2/V_1)_{max}$ | 8.70 | 9.14 | 8.84 | 8.59 | 8.95 |
| 2nd stage, $(V_3/V_1)_{max}$ | 11.99 | 11.45 | 10.22 | 10.91 | 11.13 |

[a] Other processing conditions: melt draw ratio ($V_1/V_0$), about 2; air-gap distance, 2 in.; $V_0$ = 4.76 m/min; annealing bath temperature, 100°C.

The effect of air-gap distance on the maximum stretch ratio in the cold drawing operation was investigated, and the results are summarized in Table V, showing that the effect is small. Note, in Table V, that the melt draw ratio $V_1/V_0$ was kept constant, regardless of the air-gap distance.

The effect of melt draw ratio on the maximum stretch ratio in the cold-drawing operation was investigated, and the result is summarized in Table VI. It is seen that the maximum cold stretch ratio $(V_2/V_1)_{max}$ (i.e., in the annealing bath) is lower for the filaments with the melt draw ratio of 4.02 than for the filaments with the melt draw ratio of 2.06. However, the overall maximum stretch ratio $(V_2/V_0)_{max}$ is greater for the filaments with high melt draw ratio than for the filaments with low melt draw ratio.

Table VII gives a summary of the cold-drawing operation in terms of the maximum stretch ratio for two different grades of Union Carbide high-density polyethylene (HDPE). It is seen that the maximum stretch ratio at the second

TABLE IV
The Effect of Annealing Bath Temperature on the Maximum Stretch Ratio of Mitsui High-Density Polyethylenes[a]

| Material | Maximum stretch ratio at 1st stage stretching | Annealing bath temp., °C 60 | 80 | 100 |
|---|---|---|---|---|
| Sample A | $(V_2/V_1)_{max}$ | 8.45 | 10.56 | 10.89 |
| Sample C | $(V_2/V_1)_{max}$ | 9.57 | 8.97 | 8.84 |

[a] Other processing conditions: melt draw ratio ($V_1/V_0$), about 2; air-gap distance, about 2 in.; $V_0$ = 4.81 m/min; extrusion temperature, 260°C.

TABLE V
The Effect of Air-Gap Distance on the Maximum Stretch Ratio of Mitsui High-Density Polyethylene

| Air-gap distance, in. | Maximum stretch ratio at 1st stage stretching | Annealing bath temp., °C 60 | 80 | 100 |
|---|---|---|---|---|
| 2 | $(V_2/V_1)_{max}$ | 9.57 | 8.97 | 14.68 |
| 8 | $(V_2/V_1)_{max}$ | 10.03 | 10.43 | 12.08 |

[a] Other processing conditions: melt draw ratio ($V_1/V_0$), about 2; $V_0$ = 4.81 m/min. Material is Sample C, and the extrusion temperature is 260°C.

TABLE VI
The Effect of Melt Draw Ratio on the Maximum Stretch Ratio of Mitsui High-Density Polyethylene[a]

| Melt draw ratio ($V_1/V_0$) | Cold draw ratio | Annealing bath temp., °C 60 | 80 | 100 |
|---|---|---|---|---|
| (a) Maximum Cold Draw Ratio, $(V_2/V_1)_{max}$ | | | | |
| 2.06 | $(V_2/V_1)_{max}$ | 9.57 | 8.97 | 14.68 |
| 4.02 | $(V_2/V_1)_{max}$ | 7.82 | 8.33 | 8.33 |
| (b) Maximum Overall Draw Ratio $(V_2/V_0)_{max}$ | | | | |
| Melt draw ratio ($V_1/V_0$) | Overall draw ratio | Annealing bath temp., °C 60 | 80 | 100 |
| 2.04 | $(V_2/V_0)_{max}$ | 19.71 | 18.47 | 30.24 |
| 4.02 | $(V_2/V_0)_{max}$ | 31.43 | 33.50 | 33.50 |

[a] Other processing conditions: air-gap distance, 2 in.; $V_0$ = 4.83 m/min. Material is Sample C, and the extrusion temperature is 260°C.

stage cold drawing is greater than that at the first stage cold drawing. This is very similar to that observed with Mitsui HDPE filaments (see Table II). The extrusion temperature appears to have little influence on stretchability. A clear trend is seen for the HDPE with the narrower molecular weight distribution (MWD) (DMDJ 5140) to exhibit greater maximum stretch ratios than the HDPE with the broader MWD (DMDJ 4306) (see Fig. 3). This trend is consistent with that of the Mitsui HDPE filaments. (Compare Table VII with Table II.)

Blends of Mitsui Resin A/Resin C and Union Carbide DMDJ 5140/DMDJ 4306 were melt-spun and cold-stretched. A summary of the results is presented in Figures 6 and 7. It is of interest to note that the maximum stretch ratio (hence stretchability and drawability) goes through a maximum at a certain blending ratio. An explanation for the existence of such a maximum requires examination of the microstructure of filaments.

Earlier, Han and Kim[14] reported that, in the melt spinning of blends of two incompatible polymers, spinnability goes through a maximum at a certain blending ratio. They offered an explanation for the phenomenon with the aid of photomicrographs.

TABLE VII
Summary of the Cold-Drawing Operation of Union Carbide High-Density Polyethylenes[a]

| Maximum stretch ratio | Extrusion temperature, °C 220 | 240 | 260 |
|---|---|---|---|
| (a) Union Carbide DMDJ 5140 | | | |
| 1st stage, $(V_2/V_1)_{max}$ | 10.52 | 11.33 | 11.45 |
| 2nd stage, $(V_3/V_1)_{max}$ | 14.43 | 19.89 | 15.77 |
| (b) Union Carbide DMDJ 4306 | | | |
| Maximum stretch ratio | Extrusion temperature, °C 220 | 240 | 260 |
| 1st stage, $(V_2/V_1)_{max}$ | 10.22 | 9.43 | 9.95 |
| 2nd stage, $(V_3/V_1)_{max}$ | 14.29 | 10.62 | 11.68 |

[a] Other processing conditions: melt draw ratio ($V_1/V_0$), about 2; air-gap distance, 2 in.; $V_0$ = 4.81 m/min.

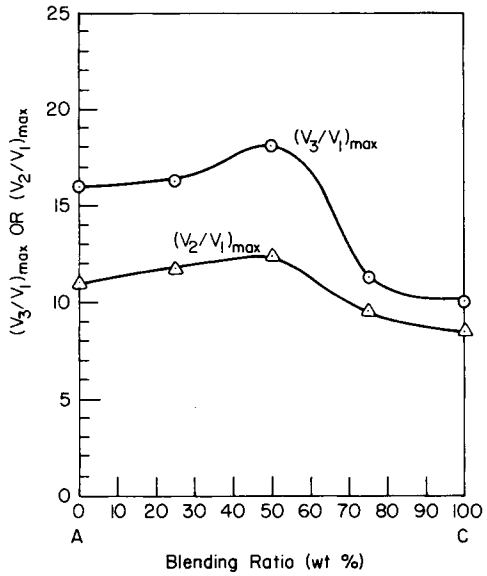


Fig. 6. Maximum cold-draw ratios for blends of Mitsui high-density polyethylenes A and B. The melt spinning temperature was 270°C, and the annealing bath temperature was 100°C.

## Filament Nonuniformity and Threadline Instability

It has been observed that a filament exhibits nonuniformity in its diameter at certain stretch ratios in the annealing bath, the so-called "necking" phenomenon. However, as the stretch ratio is increased, the nonuniform filament becomes uniform again. In other words, the thermal history of the filament, quenched, slowly cooled, or annealed, affects the draw behavior. Figures 8 and 9 show some representative photographs of filament samples collected at dif-

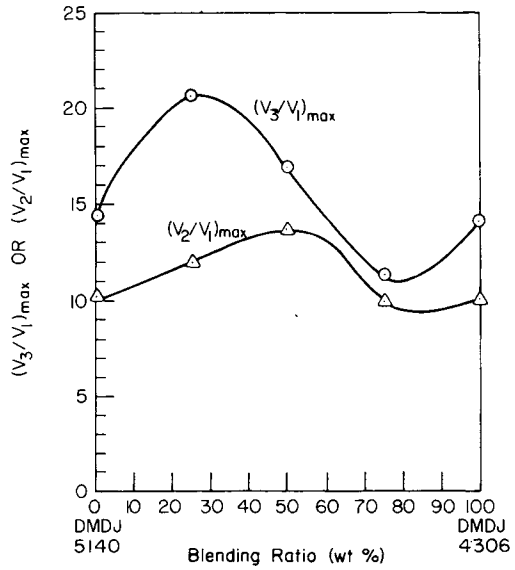


Fig. 7. Maximum cold-draw ratios for blends of Union Carbide high-density polyethylenes DMDJ 5140 and DMDJ 4306. The melt spinning temperature was 220°C, and the annealing bath temperature was 100°C.

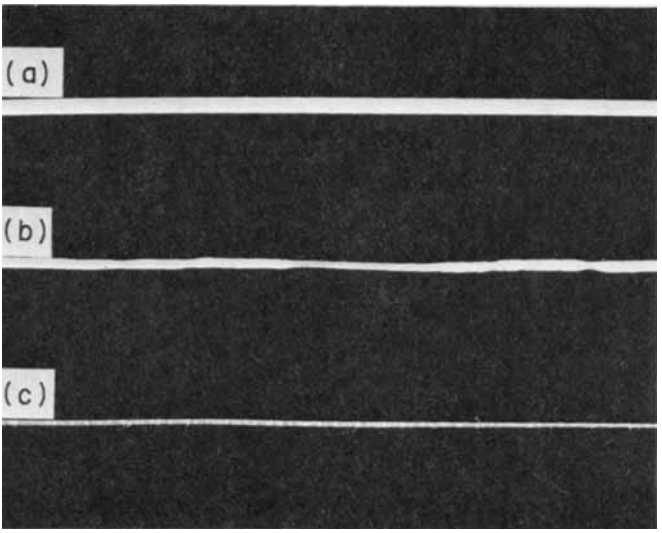


Fig. 8. Fiber samples of Mitsui high-density polyethylene (Resin A): (a) as melt-spun with a stretch ratio $V_1/V_0 = 2.12$; (b) after cold drawn with a stretch ratio $V_3/V_1 = 2.45$; (c) after cold drawn with a stretch ratio $V_3/V_1 = 11.10$.

ferent stretch ratios. In the past, interpretation of "necking" in terms of the viscoelastic flow of the amorphous phase, accompanying orientation of crystallites, has been given by Wada and Nakayama.[15] "Necking" is exhibited by most semicrystalline polymers.

A failure mechanism, known as "draw resonance," has also been observed in the present investigation. "Draw resonance" is a phenomenon of flow instability, in which a periodic pulsation occurs in the thread diameter at and above a critical value of stretch ratio,[16–20] leading eventually to thread breakage. Figure 10 gives

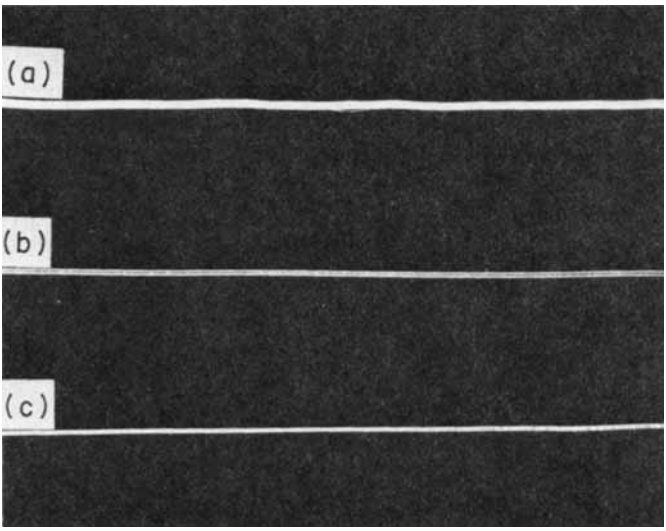


Fig. 9. Fiber samples of Union Carbide high-density polyethylene (DMDJ 4306): (a) after cold drawn with a stretch ratio $V_3/V_1 = 2.50$; (b) after cold drawn with a stretch ratio $V_3/V_1 = 6.11$; (c) after cold drawn with a stretch ratio $V_3/V_1 = 8.88$.

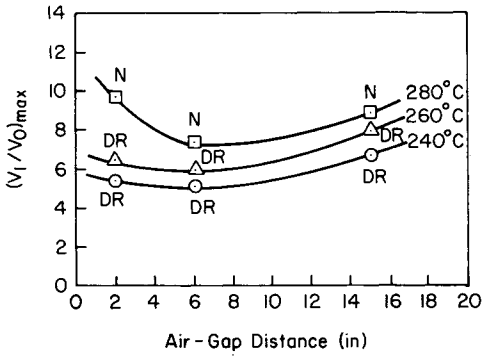


Fig. 10. Maximum melt draw ratio vs air-gap distance for Mitsui high-density polyethylene (Resin A) at different melt extrusion temperatures.

plots of the maximum melt draw ratio $(V_1/V_0)_{max}$ versus air-gap distance for Mitsui Resin A. Note that $(V_1/V_0)_{max}$ is the stretch ratio at which thread breakage occurs.

It is of interest to note in Fig. 10 that, for Mitsui Resin A, thread breakage occurs via the "draw resonance" type of instability at both 240 and 260°C (designated with the letters DR), whereas, at 280°C, thread breakage occurs via the "necking" type of instability (designated with the letter N). The other polyethylenes used (see Table I) exhibit similar failure mechanisms with respect to melt extrusion temperature. In other words, different failure mechanisms control the stability of the threadline, depending on the melt extrusion temperature. This raises a rather puzzling and as yet unresolved fundamental question concerning the origin of the two different types of failure mechanism.

In the past, fairly extensive investigations of the necking phenomenon of polyethylene have been reported from the morphological point of view,[21] from the thermodynamic point of view,[22–24] and from the rheological point of view.[15,25,26] On the other hand, very little has been studied about draw resonance from either the morphological or the thermodynamic point of view. Substantial hydrodynamic stability analyses of the draw resonance phenomenon have been reported in the recent literature.[27–32] However, such analyses are of little practical use in explaining, for instance, (a) why draw resonance tends to disappear at higher melt extrusion temperatures (see Fig. 10 and ref. 20) and (b) what role the molecular weight and its distribution play in the occurrence of draw resonance. It appears that these questions can be answered only when one investigates the structure changes occurring in polyethylene (or other polymers) during stretching operations.

## Mechanical Properties and Fiber Morphology

The mechanical properties of polymeric materials in the solid state depend not only on the chemical structure of the macromolecules but also on the thermal and mechanical treatment of the samples. This is especially true for crystallizable polymers, where pretreatment affects the relative arrangement of the macromolecular chains. In recent years, considerable effort has been spent on investigating the mechanical properties of cold-drawn polyethylenes[1,33–35] and the morphological aspects of cold-drawn films and fibers.[36–38]

For measurements of the fiber tensile properties in the present study, an Instron tensile testing machine was used. Load–elongation curves were obtained at room temperature using a fixed elongation rate. The load–elongation curves were interpreted in terms of yield stress, tensile stress, Young's (i.e., tensile) modulus, and percent elongation at break. In the calculation of tensile properties, we have used the initial cross-sectional area of the specimen.

Figure 11 gives plots of Young's modulus versus total draw ratio for melt-drawn and cold-drawn fibers, respectively, of DMDJ 5140. The melt-drawn fibers were obtained by using the conventional melt-spinning process, that is, with exclusively air cooling, and the cold-drawn fibers were obtained by using an annealing water bath at 100°C with the already melt-drawn fibers at a melt-draw ratio of $V_1/V_0 = 7.58$, where $V_0 = 4.80$ m/min. The Young's modulus given in Figure 11 was determined by the tangent to the stress–strain curve at a strain approaching zero, i.e.,

$$E = \lim_{\epsilon \to 0} (\sigma/\epsilon) \tag{1}$$

It is seen in Figure 11 that, as the draw ratio is increased, the modulus of a cold-drawn fiber increases very rapidly, whereas the modulus of a melt-drawn fiber increases very slowly. Note, for instance, that at a draw ratio of 80, the modulus of a cold-drawn fiber is almost ten times greater than that of a melt-drawn fiber.

Figure 12 gives plots of percent elongation at break versus total draw ratio for the same fiber samples as those used in Figure 11. It is seen that, as draw ratio is increased, a cold-drawn fiber shows a sharp decrease in percent elongation at break compared to a melt-drawn fiber.

It is of interest to mention at this point that Porter and co-workers[39–42] have studied the cold extrusion process of high-density polyethylene under high pressure and at a temperature below its melting point. They obtained filaments having very high tensile moduli (6–7 × $10^{11}$ dynes/cm$^2$) and attributed the im-

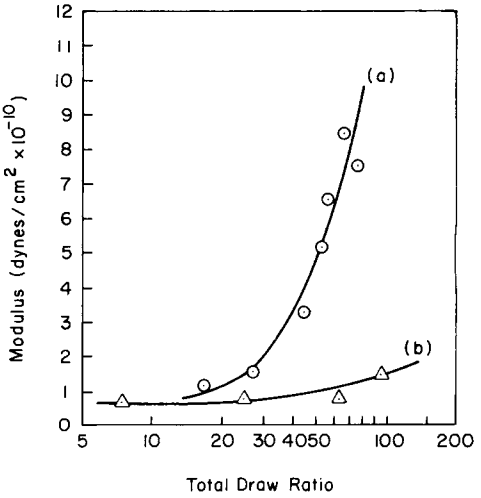


Fig. 11. Young's modulus vs total draw ratio for DMDJ 5140: (a) fiber melt drawn first with a draw ratio $V_1/V_0$ of 7.58 ($V_0 = 4.80$ m/min) and subsequently cold drawn in an annealing bath at 100°C; (b) fiber strictly melt drawn into the ambient air.

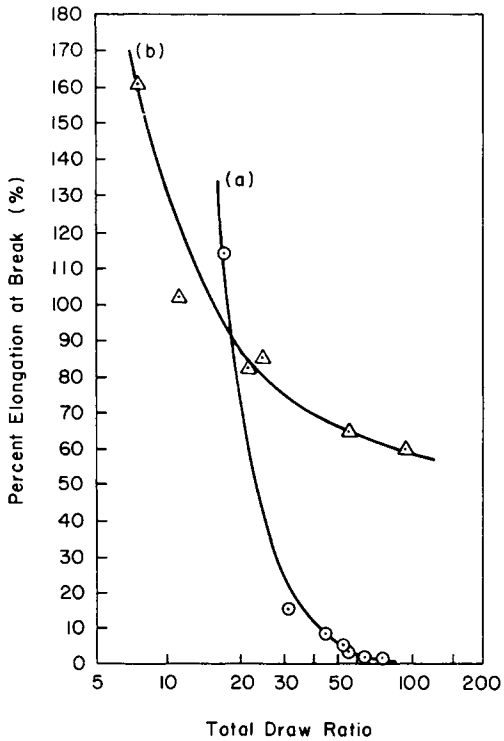


Fig. 12. Percent elongation at break vs total draw ratio for DMDJ 5140: (a) cold-drawn fiber following a mild melt drawing; (b) melt-drawn fiber.

proved properties to an increase of extended-chain crystal content (i.e., some folded-chain crystals were pulled out into extended-chain crystals).

Figure 13 gives plots of tensile modulus versus cold draw ratio of cold-drawn fibers of two Mitsui high-density polyethylenes and two Union Carbide high-density polyethylenes. The materials were first melt spun with a draw ratio of about 2, and they were subsequently cold drawn in an annealing water bath at 100°C. In view of the fact that the tensile moduli of melt-spun fibers at a draw ratio of about 2 are very low (see Fig. 11) and that all the cold-drawn fiber samples may be assumed to have had the same prestrain before they were subjected to cold drawing, we have plotted tensile modulus against cold draw ratio. It is seen in Figure 13 that the tensile modulus increases very rapidly with cold draw ratio for all the fiber samples tested. Of particular interest is the influence of molecular weight distribution on tensile modulus. Figure 13 shows clearly that the tensile modulus of broad MWD materials (Resin C and DMDJ 4306) tends to be greater than that of narrow MWD materials (Resin A and DMDJ 5140). Unfortunately, the effect of average molecular weight is not clearly separated from the effect of MWD (see Table I).

Figure 14 gives plots of elongation at break versus cold draw ratio for the same specimens as those in Figure 13. It is of interest to note in Figures 13 and 14 that the material having higher values of tensile modulus shows lower values of elongation at break, which is consistent with the observations made in reference to Figures 11 and 12. Figure 15 gives plots of tensile strength versus cold draw ratio for the same specimens as in Figures 13 and 14. It is seen that tensile

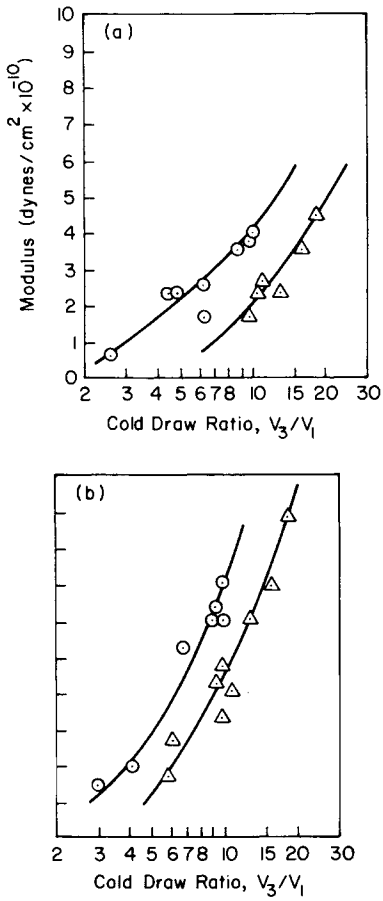


Fig. 13. Young's modulus vs cold draw ratio for (a) Mitsui high-density polyethylene with a melt draw ratio $V_1/V_0$ of 2.07 ($V_0$ = 4.81 m/min), and (b) Union Carbide high-density polyethylene with a melt draw ratio $V_1/V_0$ of 1.96 ($V_0$ = 5.10 m/min). (a) (△) Resin A; -(⊙) Resin C; (b) (△) DMDJ 5140; (⊙) DMDJ 4306.

strength increases very rapidly with cold draw ratio and that the influence of molecular weight distribution on tensile strength is *not* apparent.

Earlier, White et al.[4] have reported their observations that, as take-up velocity (i.e., melt draw ratio) was increased, both the tensile modulus and the tensile strength of melt-spun high-density polyethylene fibers increased and percent elongation at break decreased. Therefore, our observations reported above are in good agreement with their observations.

Figures 16–18 give representative results of an x-ray investigation, showing the influence of spinning conditions (i.e., take-up speed and thermal conditions) on the wide-angle x-ray diffraction patterns of the materials under test. From the x-ray patterns it may be said that the filaments are crystalline, since distinct rings are seen on the diffraction patterns. A large difference in orientation and texture is seen between the melt-drawn and cold-drawn samples. Specifically stated, the x-ray diffraction patterns of the cold-drawn samples show definite interference arcs at low draw ratios, whereas the melt-drawn samples do not show the arcs even at high draw ratios (compare Fig. 16 and Fig. 17).

Figure 19 gives plots of the $c$-axis orientation factor $f_c$ versus total draw ratio

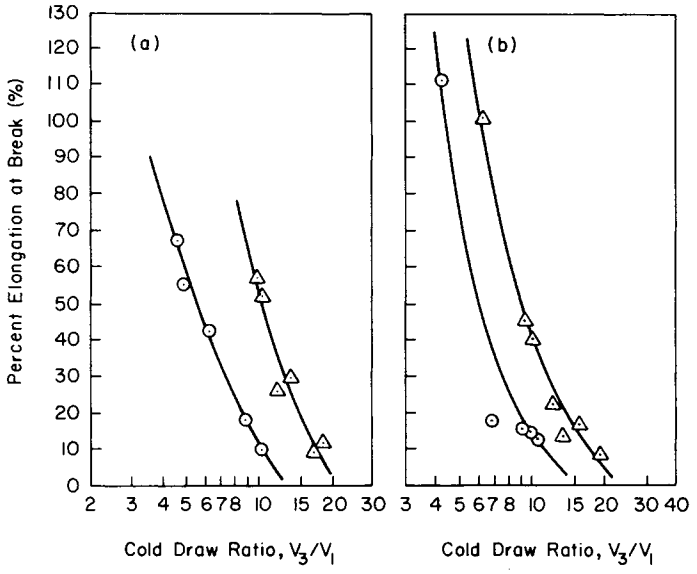


Fig. 14. Percent elongation at break vs cold draw ratio for (a) Mitsui high-density polyethylene and (b) Union Carbide high-density polyethylene. (a) (△) Resin A; (⊙) Resin C; (b) (△) DMDJ 5140; (⊙) DMDJ 4306.

from cold-drawn and melt-drawn filament samples. Here, $f_x$ (i.e., $f_a$, $f_b$, $f_c$) is the well-known Hermans orientation factor[43] defined as

$$f_x = \frac{1}{2}(3\,\overline{\cos^2\theta} - 1) \qquad -\frac{1}{2} \leq f_x \leq 1 \tag{2}$$

where $\overline{\cos^2\theta}$ is the average value of the cosine squared of the angle $\theta$ between the reference direction in the sample (fiber axis) and the x-crystallographic axis, defined as

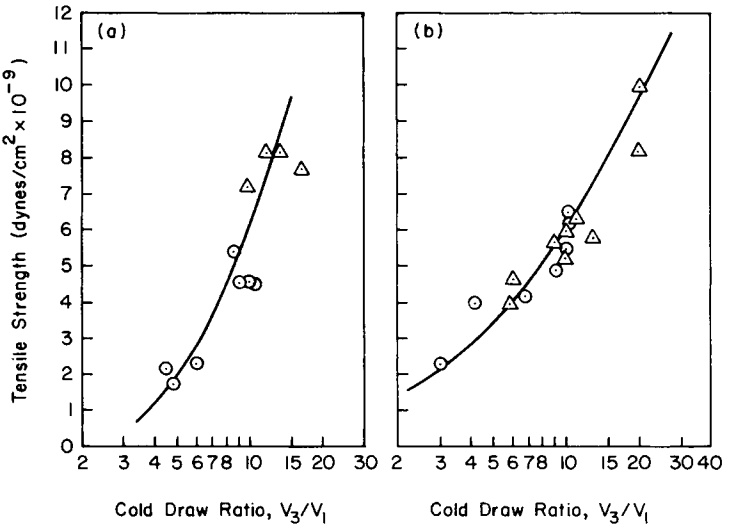


Fig. 15. Tensile strength vs cold draw ratio for (a) Mitsui high-density polyethylene and (b) Union Carbide high-density polyethylene. (a) (△) Resin A; (⊙) Resin C; (b) (△) DMDJ 5140; (⊙) DMDJ 4306.

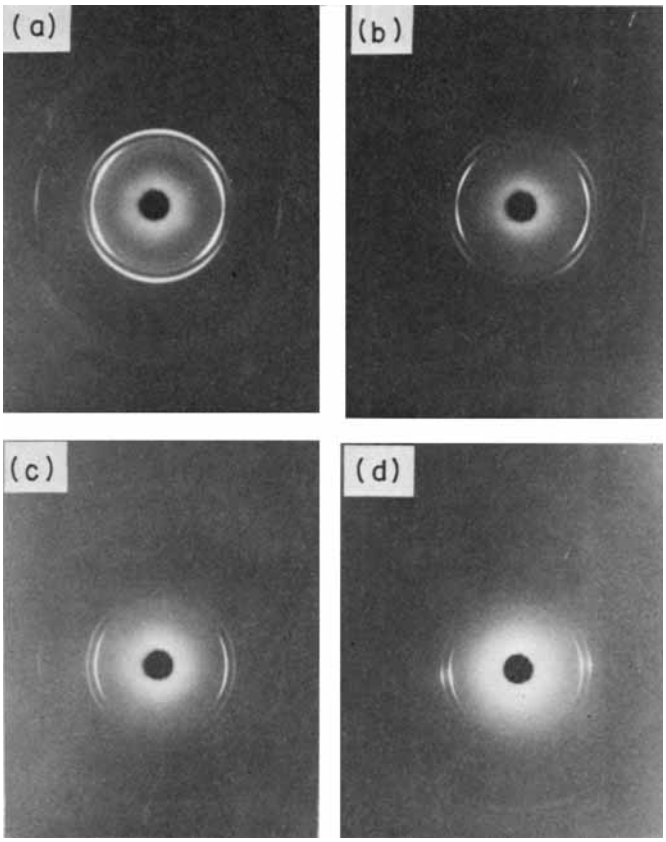


Fig. 16. Wide-angle x-ray scattering patterns of melt-drawn HDPE (DMDJ 5140) monofilaments at different draw ratios: (a) $V_1/V_0 = 7.5$; (b) $V_1/V_0 = 11.7$; (c) $V_1/V_0 = 45.1$; (d) $V_1/V_0 = 97.2$. Melt spinning conditions are: $T$ (melt temperature) = 240°C; $V_0$ = 4.80 m/min; melt spun in the quiescent air ($T$ = 20°C).

$$\overline{\cos^2\theta} = \int_0^{\pi/2} I(\theta)\cos^2\theta \sin\theta\, d\theta \Big/ \int_0^{\pi/2} I(\theta)\sin\theta\, d\theta \qquad (3)$$

in which I($\theta$) is the intensity diffraction from the plane which is perpendicular to the x-crystallographic axis.

It is seen in Figure 19 that the value of the orientation factor $f_c$ increases with draw ratio and that the cold-drawn samples give rise to greater values of $f_c$ than the melt-drawn samples.

Now, the improvements in the longitudinal Young's modulus shown in Figure 11 may be explained with the aid of Figure 19 that they may be attributable to the increased crystalline orientation caused by the increase in draw ratio. Note in Figure 11, however, that the cold-drawn samples show dramatic improvements in modulus compared to the melt-drawn samples, in particular, at draw ratios greater than 50, while the orientation factors for the two sets of samples are not much different (see Fig. 19). Note further that the great increases in modulus and tensile strength occur (see Figs. 11, 13, and 15) while the orientation factor $f_c$ remains almost unchanged at high values of draw ratio (see Fig. 19). Similar results were reported earlier by White et al.[4] Therefore, it may be concluded that the crystalline orientation alone cannot explain the dramatic improvements

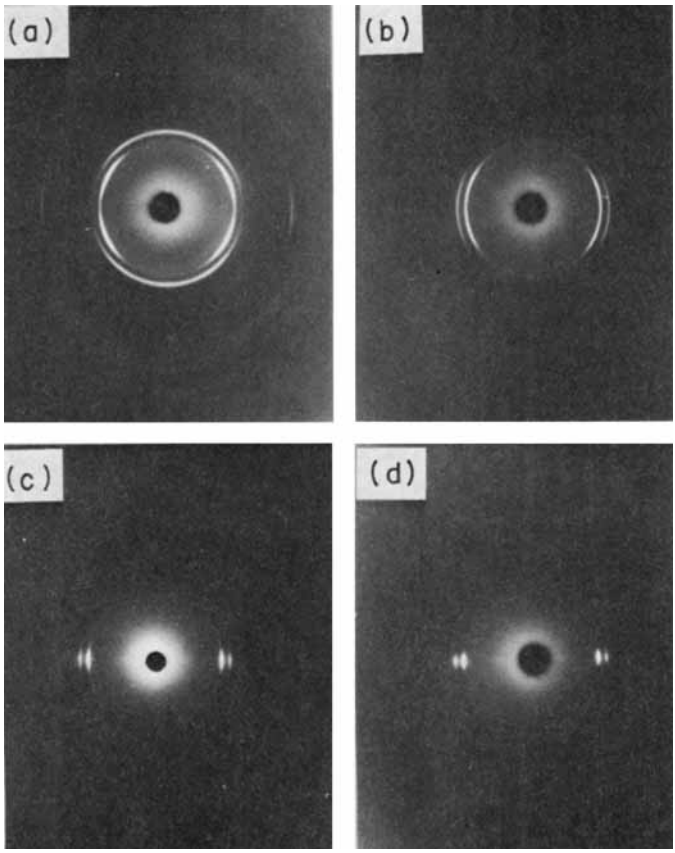


Fig. 17. Wide-angle x-ray scattering patterns of cold-drawn HDPE (DMDJ 5140) monofilaments at different draw ratios: (a) melt-drawn sample before applying cold stretching, $V_1/V_0 = 7.5$ [the same sample as that in Fig. 16(a)]; (b) cold draw ratio $V_2/V_1 = 2.3$; (c) cold draw ratio $V_2/V_1 = 6.0$; (d) cold draw ratio $V_2/V_1 = 8.0$. Other processing conditions are: $T$ (melt temperature) = 240°C; $V_0 = 4.80$ m/min; annealing bath temperature = 100°C.

in modulus of the cold-drawn samples, in particular. Cold drawing is believed to orient the molecules in the amorphous phase. In other words, the difference in the modulus between the cold- and melt-drawn samples probably resides in the orientation of the amorphous regions separating the crystalline domains rather than in the orientation of the crystalline regions.

In the past, Stein[44] studied the orientation of the crystals and the amorphous regions of polyethylene occurring during stretching, using the combined techniques of x-ray diffraction, infrared dichroism, and birefringence. Peterlin and his co-workers[34–38] studied crystal orientation and long-period of polyethylene films, using wide- and small-angle x-ray scattering. Samuels[45] has shown that crystalline and amorphous orientation parameters can be correlated with a variety of processing conditions.

The molecular weight and its distribution may affect the extent of molecular orientation under deformation. Note that the polymer having a broad MWD has higher modulus values than the polymer having a narrow MWD (see Fig. 13). In view of the existence of the correlation between the molecular orientation and the mechanical properties (e.g., modulus, tensile strength), it may be said that

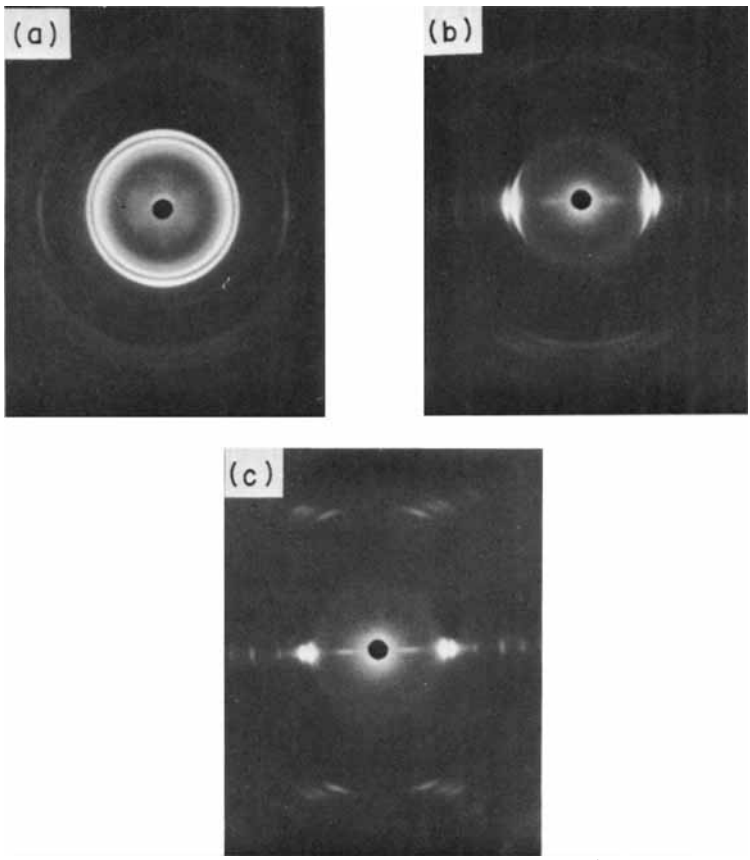


Fig. 18. Wide-angle x-ray scattering patterns of cold-drawn HDPE (Mitsui Resin C) monofilaments at different draw ratios: (a) melt-drawn sample before applying cold stretching, $V_1/V_0$ = 2.0; (b) cold drawn once, $V_2/V_1$ = 4.4; (c) cold drawn twice, $V_2/V_1$ = 4.4 (in the first-stage stretching), and $V_3/V_2$ = 2.0 (in the second-stage stretching).

the polymer having a broad MWD has greater values of the $c$-axis orientation factor than the polymer having a narrow MWD. Such an observation has indeed been reported by White et al.[4]

During fiber formation, two structural processes proceed simultaneously: crystallization and orientation along the fiber axis. The rate of crystallization and the resulting degree of crystallinity are affected by thermal conditions. Orientation also influences the rate of crystallization. On the other hand, orientation is strongly affected by the spinning conditions (e.g., draw ratio, thermal conditions) and the rate of crystallization.[46] When, under the given spinning conditions, the rate of crystallization is great compared with the rate of orientation, the structural elements that undergo orientation are the crystallites already formed. In such cases, fibers result with ordered structures, and orientation proceeds in a system of rather rigid structural elements. On the other hand, when the rate of crystallization is considerably smaller than the rate of orientation, the macromolecules do orient along the fiber axis but do not form any crystalline regions. Fibers spun under such conditions contain a large amount of the axially oriented amorphous phase.

Finally, it should be pointed out that many researchers[9,34–38,47,48] have already

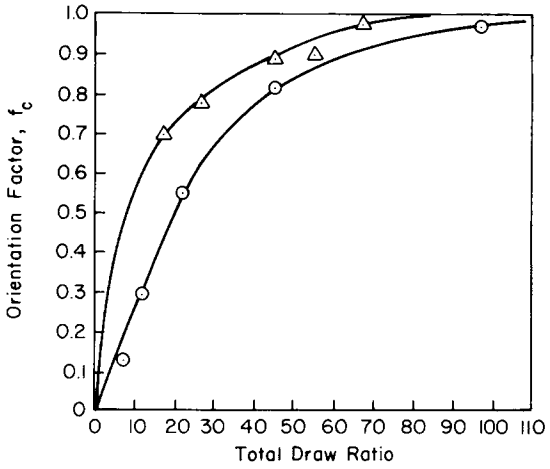


Fig. 19. The $c$-axis orientation factor for HDPE (DMDJ 5140) monofilaments as a function of draw ratio: (△) cold drawn in the annealing bath of 100°C; (⊙) melt drawn in the quiescent air ($T$ = 20°C). Other processing conditions are: $T$ (melt temperature) = 240°C; $V_0$ = 4.8 m/min.

investigated the microstructure of HDPE filaments by light and electron microscopy and by small-angle x-ray scattering.

This work was supported in part by Mitsui Petrochemical Industries, Inc., for which the authors are very grateful. They thank M. Radia for assistance in the measurement of the tensile properties of monofilament samples. Dr. N. Morosoff at Research Triangle Institute has kindly taken the time to generate the azimuthal microdensitometer traces from the wide-angle x-ray photographs, which permitted us to calculate the orientation functions of the filament samples.

## References

1. G. Meinel and A. Peterlin, *J. Polym. Sci. A-2*, **9**, 67 (1971).
2. T. D. Higgins and G. M. Bryant, *J. Appl. Polym. Sci.*, **8**, 2399 (1964).
3. L. Abbot and J. L. White, *Appl. Polym. Symp.*, **20**, 247 (1973).
4. J. L. White, K. C. Dharod, and E. S. Clark, *J. Appl. Polym. Sci.*, **18**, 2539 (1974).
5. R. Corneliussen and A. Peterlin, *Makromol. Chem.*, **105**, 193 (1967).
6. B. Cayrol and J. Peterman, *J. Polym. Sci. A-2*, **12**, 2169 (1974).
7. R. S. Stein, *J. Polym. Sci.*, **34**, 709 (1959).
8. A. Ziabicki and K. Kedzierska, *J. Appl. Polym. Sci.*, **6**, 111 (1962).
9. A. Peterlin and R. Corneliussen, *J. Polym. Sci. A-2*, **6**, 1273 (1968).
10. J. R. Dees and J. E. Spruiell, *J. Appl. Polym. Sci.*, **18**, 1053 (1974).
11. C. D. Han, *J. Appl. Polym. Sci.*, **15**, 2567 (1971).
12. C. D. Han, *Trans. Soc. Rheol.*, **18**, 163 (1974).
13. C. D. Han and R. R. Lamonte, *Trans. Soc. Rheol.*, **16**, 447 (1972).
14. C. D. Han and Y. W. Kim, *J. Appl. Polym. Sci.*, **18**, 2589 (1974).
15. Y. Wada and A. Nakayama, *J. Appl. Polym. Sci.*, **15**, 183 (1971).
16. H. I. Freeman and M. J. Coplan, *J. Appl. Polym. Sci.*, **8**, 2389 (1963).
17. A. Bergonzoni and A. J. DiCresce, *Polym. Eng. Sci.*, **6**, 45 (1966).
18. C. D. Han, R. R. Lamonte, and Y. T. Shah, *J. Appl. Polym. Sci.*, **16**, 3307 (1972).
19. C. B. Weinberger, G. F. Cruz-Saenz, and G. J. Donnelly, *A.I.Ch.E.J.*, **22**, 441 (1976).
20. C. D. Han and Y. W. Kim, *J. Appl. Polym. Sci.*, **20**, 1555 (1976).
21. N. Kasai and M. Kakudo, *J. Polym. Sci.*, **A-2**, 1955 (1964).
22. F. H. Müller, *Kolloid-Z.Z. Polym.*, **115**, 118 (1949); *ibid.*, **126**, 65 (1952).
23. F. H. Müller and K. Jäckel, *Kolloid-Z.Z. Polym.*, **129**, 145 (1952).
24. K. Jäckel, *Kolloid-Z.Z. Polym.*, **137**, 130 (1954).
25. R. E. Robertson, *J. Appl. Polym. Sci.*, **7**, 443 (1963).
26. J. C. Bauwens, C. Bauwens-Crowet, and G. Homes, *J. Polym. Sci.*, **7**, 1745 (1969).

27. J. R. A. Pearson and M. A. Matovich, *Ind. Eng. Chem., Fundam.*, **8,** 605 (1969).
28. Y. T. Shah and J. R. A. Pearson, *Ind. Eng. Chem., Fundam.*, **11,** 145 (1972).
29. Y. T. Shah and J. R. A. Pearson, *Polym. Eng. Sci.*, **12,** 219 (1972).
30. J. R. A. Pearson, Y. T. Shah, and R. D. Mhaskar, *Ind. Eng. Chem., Fundam.*, **15,** 31 (1976).
31. R. J. Fisher and M. M. Denn, *Chem. Eng. Sci.*, **30,** 1129 (1975).
32. R. J. Fisher and M. M. Denn, *A.I.Ch.E.J.*, **22,** 236 (1976).
33. R. E. Robertson, *J. Polym. Sci., Polym. Phys. Ed.*, **10,** 2437 (1972).
34. A. Peterlin, *J. Polym. Sci. C*, **15,** 427 (1966).
35. A. Peterlin, *J. Polym. Sci. A-2*, **7,** 1151 (1969).
36. A. Peterlin, *J. Mater. Sci.*, **6,** 490 (1971).
37. A. Peterlin, *Text. Res. J.*, **42,** 20 (1972).
38. G. Meinel, N. Morosoff, and A. Peterlin, *J. Polym. Sci. A-2*, **8,** 1723 (1970).
39. J. H. Southern and R. S. Porter, *J. Macromol. Sci., Phys.*, **B-4**(3), 541 (1970).
40. J. H. Southern and R. S. Porter, *J. Appl. Polym. Sci.*, **14** 2305 (1970).
41. J. H. Southern, N. E. Weeks, and R. S. Porter, *Makromol. Chem.*, **162,** 19 (1972).
42. W. G. Perkins, N. J. Capiati, and R. S. Porter, "The Effect of Molecular Weight on the Physical and Mechanical Properties of Ultra-Drawn High Density Polyethylene," Technical Report No. 3 from Polymer Science and Engineering, University of Massachusetts, Amherst, Mass., August, 1975.
43. J. J. Hermans, P. H. Hermans, D. Vermaas, and A. Weidinger, *Rec. Trav. Chim.*, **65,** 427 (1946).
44. R. S. Stein, *J. Polym. Sci.*, **31,** 327 (1958).
45. R. J. Samuels, *Structured Polymer Properties*, Wiley, New York, 1974.
46. J. E. Spruiell and J. L. White, *Polym. Eng. Sci.*, **15,** 660 (1975).
47. E. W. Fischer and G. F. Schmidt, *Angew. Chem. Int. Ed.*, **1**(9), 488 (1962).
48. J. D. Muzzy and D. Hansen, *Text. Res. J.*, **14,** 436 (1971).

Received February 16, 1977
Revised June 11, 1977